2009

Automatic Mass Balancing of Air-Bearing based Three-Axis Rotational Spacecraft Simulator

Kim, J.J.; Agrawal, B.N.

AIAA Journal of Guidance, Control, and Dynamics, Vol. 32, No. 3, May-June 2009, pp. 1005-1017.
https://hdl.handle.net/10945/34504

JOURNAL OF GUIDANCE, CONTROL, AND DYNAMICS
Vol. 32, No. 3, May–June 2009

Automatic Mass Balancing of Air-Bearing-Based Three-Axis Rotational Spacecraft Simulator

Jae Jun Kim* and Brij N. Agrawal†
Naval Postgraduate School, Monterey, California 93943

DOI: 10.2514/1.34437

Air-bearing-based spacecraft simulators are widely used to develop and verify spacecraft control techniques required by modern spacecraft applications. To create a spacelike environment with ground spacecraft simulators, the effects of gravity should be minimized. For a spherical air-bearing system with 3 rotational degrees of freedom, the center of rotation of the spacecraft simulator should be exactly aligned with the center of gravity. This paper presents the automatic mass balancing method, which compensates for the center of gravity offset from the center of rotation by actuating three proof masses on linear motion stages. Adaptive control of the automatic mass balancing system is used while the balancing masses are actuated in real time. The proposed techniques are implemented on the ground-based three-axis spacecraft simulator for the bifocal relay mirror spacecraft.

I. Introduction

GROUND simulation and testing of spacecraft dynamics is highly desirable because it is extremely difficult to test and reconfigure the system once the vehicle is in space. Rigorous ground testing of spacecraft dynamics will significantly reduce various risks to the project. Ground-based spacecraft simulators often use air bearings to simulate frictionless and microgravity space environments. Various air-bearing-based spacecraft simulators have been developed in the past ([1–16]), and a historical review is presented in [17]. Planar air-bearing systems use a set of air pads mounted under the test article to achieve frictionless sliding over a smooth surface. The planar air-bearing systems are capable of providing 1 rotational and 2 translational degrees of freedom and they are often used for simulations of formation flying, rendezvous, and docking. However, spherical air-bearing systems are often preferred for spacecraft attitude dynamics and control simulations because of their capability of providing a full 3 degrees of freedom rotational motion.

Despite the advantage of creating a nearly frictionless test platform with the air-bearing systems, there are various disturbance elements with the air-bearing-based simulators which limit perfect reproduction of the space environment. According to [18], the disturbance torques are divided into four categories: torques arising from the platform, torques from the air bearing, torques from the environment, and torques from the test system. A gravitational disturbance is created by the unbalance of the platform. The gravitational disturbance is not a concern for planar systems as long as the sliding surface is perpendicular to the direction of the gravitational acceleration. Spherical air-bearing-based spacecraft simulators, however, require the center of gravity to be precisely aligned with the center of rotation of the spacecraft. When the center of gravity is located below the center of rotation, the spherical air-bearing test bed behaves similar to a pendulum system. Because the pendulum system has a stable equilibrium point when the center of gravity is located along the gravity vector, the balance of the system cannot be guaranteed just by observing the simulator maintaining one fixed attitude. According to [1] and the authors' experience, the most effective way for manual balancing is to balance two horizontal axes first by inspecting the simulator tilt at the equilibrium point, then raising the vertical balance mass until the period of the pendulum motion becomes very large. As the center of gravity approaches close to the center of rotation by raising the vertical balance mass, checking the pendulum motion becomes difficult due to the rotational travel limit of the spacecraft simulator. Therefore, manual balancing of the simulator is a time-consuming process with limited accuracy.

To overcome the difficulties associated with the manual balancing, automatic mass balancing systems have been considered in many references [2–13]. In fact, many recently built spacecraft simulators either employ automatic mass balancing systems already [2–5] or plan to upgrade in the future [14]. The automatic mass balancing system is composed of three proof masses on three individual linear stages, which can alter their positions relative to the spacecraft body. Small and Zajac [6] presented a linear control design in which a computer simulated automatic mass balancing system reduced the external torque to within $0.0005\ \mathrm{N \cdot m}$, but the maximum unbalance torque of $0.001\ \mathrm{N \cdot m}$ is sufficient for typical attitude control system experiments. In this approach, the horizontal plane is balanced first by actuating the two masses along the two axes on the plane. Then the mass translating along the vertical axis is used to balance the simulator with a 20 deg tilt. This procedure is repeated for the balancing of the horizontal plane. The controller is designed based on the positional error from the initial position. The cross coupling between axes is ignored. Hatcher and Young [7] performed an experiment on automatic balancing by adjusting the position of the balance mass based on the differences in the actuator torque for each axis during limit-cycle operation. The balancing results showed a maximum disturbance torque of $0.001\ \mathrm{N \cdot m}$ with the average of $0.0003\ \mathrm{N \cdot m}$.

Direct estimation of the center of gravity is also frequently considered for automatic mass balancing. From the center of gravity estimation, displacement of the balance masses for compensation of unbalance can be determined. Batch estimation techniques are presented in [12,15,19–21], where a least-squares estimation is used to determine unknown parameters including the inertia matrix and the center of gravity. Various formulations of least-squares estimation can be considered such as the torque method [19], the momentum integral method [19], the filtering method [20], and the energy balance method [21,22]. Another method to determine the center of gravity is presented in [2], which is recording a set of the spacecraft's state equilibrium points for different locations of the balance masses. Because these equilibrium points indicate that the center of gravity is located along the gravity vector, the relationship between the known set of balance-mass positions and

Presented as Paper 6595 at the AIAA Guidance, Navigation, and Control Conference and Exhibit, Keystone, Colorado, 21–24 August 2006; received 4 September 2007; revision received 13 August 2008; accepted for publication 6 October 2008.

*Research Assistant Professor, Department of Mechanical and Astronautical Engineering. Member AIAA.
†Distinguished Professor, Department of Mechanical and Astronautical Engineering. Fellow AIAA.

the resulting equilibrium points can be used to estimate the location of the center of gravity. To achieve better balancing results from the batch estimation methods, it is desirable to repeat the estimation and compensation process until satisfactory balancing is achieved. The batch estimation methods can be thus time consuming. Although recursive estimation techniques using the extended Kalman filter [23] and the recursive least-squares algorithm [16] were proposed for the center of gravity estimation, actuation of the balance masses during recursive estimation was not considered due to convergence and stability problems.

Static unbalance is not the only source of gravitational disturbance on the spacecraft simulator. Because of the rotating and moving parts, flexible cables, deformation of structures (sagging), and vibration of flexible structures, spacecraft simulators also suffer from dynamic unbalance. There are other sources of disturbances including disturbances from the surrounding environments such as air currents, air damping, magnetic fields, and radiation pressure [18]. These are inherently present for ground-based spacecraft simulators. Therefore, verification of mass balancing results is a challenging task. Even considering static unbalance only, gravitational disturbance varies depending on the attitude of a spacecraft. To determine the maximum and average disturbance torque of the spacecraft simulator, inspection of disturbance torques is required at all possible combinations of spacecraft attitude, angular/linear position of rotating/translating parts, maneuver rates, etc., which is impossible to do. It is suggested in [8,13] to evaluate the effectiveness of the automatic balancing procedure by observing the oscillation period of the simulator. Although this method can provide the magnitude of the unbalance, the simulator should be able to rotate freely in any direction in order to inspect the oscillation period from a certain unbalance. Because most air-bearing-based simulators have at least one axis with a rotational travel limit, it is not possible to determine the oscillation period for all cases. In addition, dynamic unbalance and other external disturbances can affect the period of the pendulum motion.

In this paper, a rigid-body spacecraft simulator equipped with momentum exchange devices is used as a mathematical model. This model has a nonlinear coupling between the three axes of the spacecraft. An automatic mass balancing system is first introduced and the relationship between the balance-mass actuation and the center of gravity shift is determined. A batch estimation method for the inertia matrix and the center of gravity is presented as a first step for automatic mass balancing. This batch estimation method is based on the integrated form of the torque method presented in [19] and used as a base method for automatic mass balancing. The adaptive control method for the automatic mass balancing system is presented next. The first idea is to actuate the balance masses in the direction along which the total angular momentum of the spacecraft simulator becomes constant, which is equivalent to zero external torque. The result of this method will drive the spacecraft simulator toward an equilibrium point of a pendulum motion with incorrect center of gravity compensation as explained later. To solve this problem, the spacecraft simulator is excited persistently with a preplanned spacecraft momentum trajectory. The balance masses are actuated toward the direction where the error between the actual and preplanned momentum trajectories become zero. Any gravitational disturbance by the unbalance is eliminated from the proposed design for the spacecraft simulator represented by the aforementioned mathematical model.

To verify the adaptive automatic balancing control design, experimental results are also included in the paper. The air-bearing-based three-axis spacecraft simulator developed at the Naval Postgraduate School (NPS) is used for experiments. This spacecraft simulator is a second generation air-bearing test bed developed at the NPS to demonstrate the operation of the bifocal relay mirror spacecraft (BRMS). The adaptive automatic mass balancing method is based on the mathematical model that accounts for static unbalance only, whereas the actual spacecraft simulator suffers also from dynamic unbalance, various disturbances, and sensor/actuator errors. The discussion of the experimental results is presented to evaluate the effectiveness of the adaptive mass balancing control method for the actual system and to identify the future improvements for various applications of automatic mass balancing systems.

II. Automatic Mass Balancing System

An automatic mass balancing system is typically composed of three moving balance masses on linear stages as illustrated in Fig. 1. The three balance masses move along the unit vector directions represented by $\mathbf{u}_1$, $\mathbf{u}_2$, and $\mathbf{u}_3$. In Fig. 1, these unit vectors are located parallel to the three axes of the spacecraft body. This is not a requirement for the mass balancing system as long as the net displacement of the balance masses can create a three-dimensional mass shift. The endpoints of the vectors, $\boldsymbol{\rho}_1$, $\boldsymbol{\rho}_2$, and $\boldsymbol{\rho}_3$, represent the zero locations of the balance masses. The balance-mass displacements d_1, d_2, and d_3 are referenced from these zero locations. The location vector of each balance mass represented in the spacecraft body frame centered at O can be written as

$$\mathbf{R}_i = \boldsymbol{\rho}_i + d_i \mathbf{u}_i \qquad (i = 1 \cdots 3) \tag{1}$$

The center of gravity vector $\mathbf{r}$ is computed as

$$\mathbf{r} = \frac{1}{m}\int_B R\,\mathrm{d}m = \frac{1}{m}\left[(m - m_B)\mathbf{R}_0 + \sum_{i=1}^{3} m_i \mathbf{R}_i\right] \tag{2}$$

where m is the total mass of the spacecraft including balance masses, $m_B = m_1 + m_2 + m_3$ represents the sum of balance masses, and $\mathbf{R}_0$ is the center of gravity vector without balance masses. When the spacecraft simulator is perfectly balanced, $\mathbf{r}$ is a zero vector. When the balance masses are moved by Δd_i $(i = 1 \cdots 3)$, the new location of the center of mass becomes

$$\mathbf{r}' = \frac{1}{m}\left[(m - m_B)\mathbf{R}_0 + \sum_{i=1}^{3} m_i(\boldsymbol{\rho}_i + (d_i + \Delta d_i)\mathbf{u}_i)\right] \tag{3}$$

The change in the center of mass vector becomes

$$\Delta\mathbf{r} = \mathbf{r}' - \mathbf{r} = \frac{1}{m}\sum_{i=1}^{3} m_i \Delta d_i \mathbf{u}_i \tag{4}$$

We define the estimated center of gravity vector of the spacecraft including the balance masses as $\hat{\mathbf{r}}$. To compensate for the center of gravity offset of $\hat{\mathbf{r}}$, $\Delta\mathbf{r}$ in Eq. (4) should be equal to $-\hat{\mathbf{r}}$. Substituting $\Delta\mathbf{r} = -\hat{\mathbf{r}}$ and solving for Δd_i yields

$$\Delta\mathbf{d} = -[\,m_1\mathbf{u}_1 \quad m_2\mathbf{u}_2 \quad m_3\mathbf{u}_3\,]^{-1} m\hat{\mathbf{r}} \tag{5}$$

where $\Delta\mathbf{d} = [\,\Delta d_1 \quad \Delta d_2 \quad \Delta d_3\,]^T$. When the three balance masses are aligned along the three spacecraft body axes as shown in Fig. 1, Eq. (5) can also be written as

$$\Delta\mathbf{d} = -\mathrm{diag}\left(\frac{1}{m_1}, \frac{1}{m_2}, \frac{1}{m_3}\right) m\hat{\mathbf{r}} \tag{6}$$

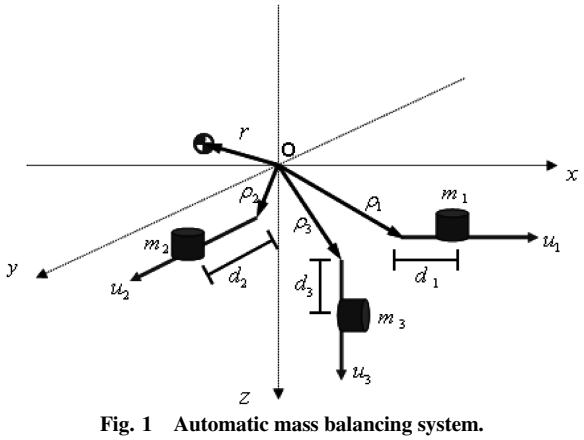

Fig. 1 Automatic mass balancing system.

where diag( ) represents a diagonal matrix. If the correct center of gravity vector is estimated, the static unbalance of the spacecraft simulator can be eliminated using Eq. (6). It should be noted that the exact mass of the spacecraft simulator is also required in Eq. (6) for correct compensation of the center of gravity offset. The exact mass of the spacecraft simulator is difficult to measure because spacecraft simulators are usually quite heavy. Therefore, it is better to include the mass of the simulator and estimate the combined value ($m\mathbf{r}$).

The inertia of the spacecraft is also altered as a result of the center of mass offset correction. We define the estimated inertia of the spacecraft simulator before the correction of the center of gravity offset as $\hat{J}$. This inertia matrix can be broken into two parts as

$$\hat{J} = \hat{J}_s + \sum_{i=1}^{3}(-m_i[\mathbf{R}_i\times][\mathbf{R}_i\times]) \tag{7}$$

where $\hat{J}_s$ stands for the estimated inertia matrix without balancing masses and $[\mathbf{R}_i\times]$ is a cross-product matrix corresponding to the position vector of the ith balance mass, where the cross-product matrix is defined by the following relationship:

$$[\mathbf{a}\times] = \begin{bmatrix} 0 & -a_3 & a_2 \\ a_3 & 0 & -a_1 \\ -a_2 & a_1 & 0 \end{bmatrix}, \qquad \mathbf{a} = \begin{bmatrix} a_1 \\ a_2 \\ a_3 \end{bmatrix} \tag{8}$$

The new inertia matrix after the center of mass offset compensation becomes

$$\hat{J}' = \hat{J} - \sum_{i=1}^{3}(-m_i[\mathbf{R}_i\times][\mathbf{R}_i\times]) + \sum_{i=1}^{3}(-m_i[\mathbf{R}_i'\times][\mathbf{R}_i'\times]) \tag{9}$$

where

$$\mathbf{R}_i' = (\boldsymbol{\rho}_i + (d_i + \Delta d_i)\mathbf{u}_i) \tag{10}$$

III. Batch Estimation of the Center of Gravity

In this paper, a rigid-body three-axis spacecraft simulator with momentum exchange devices is considered. A simple equation describing the dynamics of the spacecraft simulator in the spacecraft body-fixed coordinates is written as

$$J\dot{\omega} + \omega \times J\omega = -\dot{\mathbf{h}} - \omega \times \mathbf{h} + \mathbf{r} \times m\mathbf{g} \tag{11}$$

where J is the total moment of inertia including the momentum exchange devices, ω is the angular rate of the spacecraft, $\mathbf{h}$ is the total momentum of the momentum exchange devices, m is the total mass, $\mathbf{r}$ is a constant vector from the center of rotation to the center of gravity (center of gravity vector in spacecraft body frame), and $\mathbf{g}$ is the gravitational acceleration vector. The unknowns to be estimated in Eq. (11) are the inertia matrix J and the mass of the spacecraft simulator times the center of mass vector, $m\mathbf{r}$. Defining the matrix Ω and the vector of inertia matrix elements $\tilde{\mathbf{J}}$ as

$$\Omega = \begin{bmatrix} \omega_1 & 0 & 0 & \omega_2 & \omega_3 & 0 \\ 0 & \omega_2 & 0 & \omega_1 & 0 & \omega_3 \\ 0 & 0 & \omega_3 & 0 & \omega_1 & \omega_2 \end{bmatrix}$$
$$\tilde{\mathbf{J}} = [J_{xx} \quad J_{yy} \quad J_{zz} \quad J_{xy} \quad J_{xz} \quad J_{yz}]^T \tag{12}$$

Equation (11) can be rewritten as

$$\dot{\Omega}\,\tilde{\mathbf{J}} + \omega \times \Omega\tilde{\mathbf{J}} = -\dot{\mathbf{h}} - \omega \times \mathbf{h} - [\mathbf{g}\times]m\mathbf{r} \tag{13}$$

Equation (13) may be written in matrix form, which is also done in [2]:

$$[\,\dot{\Omega} + \omega \times \Omega \quad [\mathbf{g}\times]\,]\begin{bmatrix} \tilde{\mathbf{J}} \\ m\mathbf{r} \end{bmatrix} = -\dot{\mathbf{h}} - \omega \times \mathbf{h} \tag{14}$$

Equation (14) requires the knowledge of $\dot{\omega}$ which requires numerical differentiation of the rate gyro signals. Therefore, direct application of the least-squares method is not desired. In this paper, simple integration of Eq. (14) is used as follows:

$$\begin{bmatrix} \Omega + \int_{t_0}^{t}([\omega\times]\Omega)\,\mathrm{d}t & \int_{t_0}^{t}[\mathbf{g}\times]\,\mathrm{d}t \end{bmatrix}\begin{bmatrix} \tilde{\mathbf{J}} \\ m\mathbf{r} \end{bmatrix} = -\mathbf{h} - \int_{t_0}^{t}(\omega \times \mathbf{h})\,\mathrm{d}t \tag{15}$$

Equation (15) is in the form of a linear equation $\phi\mathbf{x} = y$, where $\mathbf{x} = [\,\tilde{\mathbf{J}} \quad m\mathbf{r}\,]^T$ is the unknown vector to be estimated. The standard form of the least-squares problem becomes $\Phi\mathbf{x} = \mathbf{y}$, where

$$\Phi = \begin{bmatrix} \phi(t = t_0) \\ \phi(t = t_1) \\ \vdots \\ \phi(t = t_n) \end{bmatrix}, \qquad \mathbf{y} = \begin{bmatrix} y(t = t_0) \\ y(t = t_1) \\ \vdots \\ y(t = t_n) \end{bmatrix} \tag{16}$$

Then the least-squares solution becomes $\mathbf{x} = (\boldsymbol{\Phi}^T\boldsymbol{\Phi})^{-1}\boldsymbol{\Phi}^T\mathbf{y}$. The resulting estimated values of $m\mathbf{r}$ can be directly used for compensation of the center of gravity vector using the following equation:

$$\Delta\mathbf{d} = -\mathrm{diag}\left(\frac{1}{m_1}, \frac{1}{m_2}, \frac{1}{m_3}\right)\widehat{m\mathbf{r}} \tag{17}$$

where $\widehat{m\mathbf{r}}$ denotes the estimated value of the simulator mass times the center of gravity vector.

IV. Adaptive Control of the Automatic Mass Balancing System

The batch estimation technique discussed in the previous section requires accurate estimation of parameters for compensation of the center of gravity offset. Because of various reasons including inaccurate mass values and locations of balance masses, sensor and actuator errors, dynamic unbalance, and environmental disturbances, the compensation result may not yield a required gravity-free simulation environment level with just a single batch estimation. To avoid repeated batch estimations for improved balancing results, an adaptive control method with the online actuation of the automatic mass balancing system is proposed. The proposed method assumes that the estimate of the spacecraft inertia is initially available. The inertia of the spacecraft simulator can be estimated using the method presented in the previous section. The equation of motion for a spacecraft simulator in body-fixed coordinates can be written as

$$\dot{\mathbf{H}} + [\omega\times]\mathbf{H} = m(\mathbf{r} \times \mathbf{g}) \tag{18}$$

where the time-varying center of mass vector $\mathbf{r}(t)$ can be written as

$$\mathbf{r}\,(t) = \mathbf{r}_0 + \delta\mathbf{r}(t) \tag{19}$$

$\mathbf{H}$ represents total momentum of a spacecraft simulator, $\mathbf{r}_0$ represents the center of mass location vector at time zero, and $\delta\mathbf{r}$ is the change of the center of mass due to the automatic mass balancing actuation. The problem consists of actuating the balance masses so that the compensation for the unknown $\mathbf{r}_0$ is achieved. When the simulator is perfectly balanced, $\delta\mathbf{r}$ becomes $-\mathbf{r}_0$ such that $\mathbf{r} = \mathbf{r}_0 + \delta\mathbf{r} = 0$. The total momentum in Eq. (18) is written as

$$\mathbf{H} = J\omega + \sum_{i=1}^{3}\mathbf{R}_i \times m_i\dot{\mathbf{R}}_i + \mathbf{h} \tag{20}$$

where $\mathbf{h}$ is the momentum of the momentum exchange device. Note that the spacecraft inertia matrix (J) is now time varying and is determined by the balance-mass positions. The inertia of the spacecraft without balancing masses can be written as

$$J_s = J(0) - \sum_{i=1}^{3}(-m_i[\mathbf{R}_i(0)\times][\mathbf{R}_i(0)\times]) \tag{21}$$

Then the inertia matrix at time t can be computed as

$$J(t) = J_s + \sum_{i=1}^{3}(-m_i[\mathbf{R}_i(t)\times][\mathbf{R}_i(t)\times]) \tag{22}$$

The spacecraft equation of motion in Eq. (18) can be further written as

$$\dot{\mathbf{H}}_s + [\omega\times]\mathbf{H}_s = \tau - m[\mathbf{g}\times](\mathbf{r}_0 + \delta\mathbf{r}) \tag{23}$$

where

$$\mathbf{H}_s = J\omega + \sum_{i=1}^{3}\mathbf{R}_i \times m_i\dot{\mathbf{R}}_i, \qquad \tau = -\dot{\mathbf{h}} - [\omega\times]h \tag{24}$$

Proposing the feedback control law as $\tau = (-K + [\omega\times])\mathbf{H}_s$ with symmetric positive definite matrix K, the closed-loop equation of motion becomes

$$\dot{\mathbf{H}}_s + K\mathbf{H}_s = -m[\mathbf{g}\times](\mathbf{r_0} + \delta\mathbf{r}) \tag{25}$$

We define the candidate Lyapunov function as

$$V(\mathbf{H}_s, \delta\mathbf{r}) = \tfrac{1}{2}\mathbf{H}_s^T\mathbf{H}_s + \tfrac{1}{2}(\mathbf{r}_0 + \delta\mathbf{r})^T\Gamma^{-1}(\mathbf{r}_0 + \delta\mathbf{r}) \tag{26}$$

where Γ is a symmetric positive definite matrix. The time derivative of the candidate Lyapunov function becomes

$$\begin{aligned}\dot{V} &= \mathbf{H}_s^T\dot{\mathbf{H}}_s + (\mathbf{r}_0 + \delta\mathbf{r})^T\Gamma^{-1}\dot{\delta}\mathbf{r} \\ &= \mathbf{H}_s^T[-K\mathbf{H}_s - m[\mathbf{g}\times](\mathbf{r} + \delta\mathbf{r})] + (\mathbf{r}_0 + \delta\mathbf{r})^T\Gamma^{-1}\dot{\delta}\mathbf{r}\end{aligned} \tag{27}$$

The adaptation rule is chosen as

$$\dot{\delta}\mathbf{r} = m\Gamma[\mathbf{g}\times]^T\mathbf{H}_s \tag{28}$$

The adaptation rule can be further written as a function of the positions of the mass balancers for implementation purposes. It can be shown that

$$\delta\mathbf{r} = \frac{1}{m}\sum_{i=1}^{3} m_i\delta d_i\mathbf{u}_i = \frac{1}{m}G\delta\mathbf{d} \tag{29}$$

where $\delta\mathbf{d} = [\,\delta d_1 \quad \delta d_2 \quad \delta d_3\,]^T$ and $G = [\,m_1\mathbf{u}_1 \quad m_2\mathbf{u}_2 \quad m_3\mathbf{u}_3\,]$. The time derivative of the equation yields

$$\dot{\delta}\mathbf{r} = \frac{1}{m}G\dot{\delta}\mathbf{d} \tag{30}$$

Then the adaptation rule becomes

$$\dot{\delta}\mathbf{d} = m^2G^{-1}\Gamma[\mathbf{g}\times]^T\mathbf{H}_s \tag{31}$$

The time derivative of the candidate Lyapunov function with the proposed adaptation rule becomes

$$\dot{V} = -\mathbf{H}_s^TK\mathbf{H}_s \tag{32}$$

which is negative semidefinite. Since $\delta\mathbf{r}$ and τ are bounded, $\dot{\mathbf{H}}_s$ is also bounded. The derivative of $\dot{V}$ is

$$\ddot{V} = -2\mathbf{H}_s^TK\dot{\mathbf{H}}_s \tag{33}$$

which is also bounded. Therefore, the momentum $\mathbf{H}_s$ is stable and goes to zero as time goes to infinity. Because the momentum $\mathbf{H}_s$ goes to zero, the control input τ and mass balancing actuation $\dot{\delta}\mathbf{r}$ also become zero. This indicates that the total angular momentum

$$\mathbf{H} = J\omega + \sum_{i=1}^{3}\mathbf{R}_i \times m_i\dot{\mathbf{R}}_i + \mathbf{h}$$

becomes constant in the end.

Although the total angular momentum will be conserved eventually with the proposed control method, it is not sufficient for balancing the system. There exists a state where total angular momentum is conserved even when the center of mass does not coincide with the center of rotation. Because the rank of the skew symmetric matrix $[\mathbf{g}\times]$ is always 2, there exists a null vector solution that makes the gravitational torque zero such that $[\mathbf{g}\times]m(\mathbf{r_0} + \delta\mathbf{r}) = \mathbf{0}$. From the following equation, any real k will not affect the motion of the spacecraft simulator since $[\mathbf{g}\times]k\mathbf{g} = 0$,

$$\dot{\mathbf{H}}_s + [\omega\times]\mathbf{H}_s = \tau - m[\mathbf{g}\times](\mathbf{r}_0 + \delta\mathbf{r} + k\mathbf{g}) \tag{34}$$

This corresponds to a situation where the center of mass is located along the gravity vector as shown in Fig. 2. The system will be in the equilibrium state with the center of mass located along the gravity vector as a result. To ensure balancing in any state, the simulator needs to maneuver constantly. The simplest solution is to generate a desired spacecraft momentum trajectory that can provide persistent maneuvering of the spacecraft simulator. We define the desired spacecraft momentum trajectory to be $\mathbf{H}_d$. Proposing the candidate Lyapunov function as

$$V(\mathbf{H}_s, \delta\mathbf{r}) = \tfrac{1}{2}(\mathbf{H}_s - \mathbf{H}_d)^T(\mathbf{H}_s - \mathbf{H}_d) + \tfrac{1}{2}(\mathbf{r}_0 + \delta\mathbf{r})^T\Gamma^{-1}(\mathbf{r}_0 + \delta\mathbf{r}) \tag{35}$$

the time derivative of the candidate Lyapunov function becomes

$$\dot{V} = (\mathbf{H}_s - \mathbf{H}_d)^T(\dot{\mathbf{H}}_s - \dot{\mathbf{H}}_d) + (\mathbf{r}_0 + \delta\mathbf{r})\Gamma^{-1}\dot{\delta}\mathbf{r} \tag{36}$$

The combined feedback and feedforward momentum tracking control law is proposed as

$$\tau = -K(\mathbf{H}_s - \mathbf{H}_d) + [\omega\times]\mathbf{H}_s + \dot{\mathbf{H}}_d \tag{37}$$

The time derivative of the candidate Lyapunov function becomes

$$\begin{aligned}\dot{V} = (\mathbf{H}_s - \mathbf{H}_d)^T[&-K(\mathbf{H}_s - \mathbf{H}_d) \\ &- [\mathbf{g}\times]m(\mathbf{r}_0 - \delta\mathbf{r})] + (\mathbf{r}_0 + \delta\mathbf{r})\Gamma^{-1}\dot{\delta}\mathbf{r}\end{aligned} \tag{38}$$

Let the adaptation law be

$$\dot{\delta}\mathbf{r} = m\Gamma[\mathbf{g}\times]^T(\mathbf{H}_s - \mathbf{H}_d)$$

or equivalently

$$\dot{\delta}\mathbf{d} = m^2G^{-1}\Gamma[\mathbf{g}\times]^T(\mathbf{H}_s - \mathbf{H}_d) \tag{39}$$

Then, the time derivative of the candidate Lyapunov function becomes

$$\dot{V} = -(\mathbf{H}_s - \mathbf{H}_d)^TK(\mathbf{H}_s - \mathbf{H}_d) \tag{40}$$

It can also be shown that the spacecraft momentum tracking error becomes zero as time goes to infinity. When the tracking error becomes zero, $\mathbf{H}_s$ converges to $\mathbf{H}_d$ and the external gravitational disturbance torque becomes zero. Because the spacecraft is constantly maneuvering, the center of gravity also converges to zero to have a zero gravitational disturbance torque.

To verify the proposed control law, a computer simulation is developed. The top two plots in Fig. 3 show the results of the adaptive

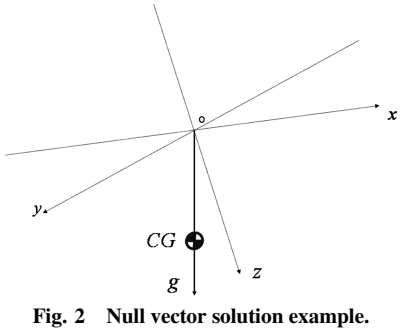

Fig. 2 Null vector solution example.

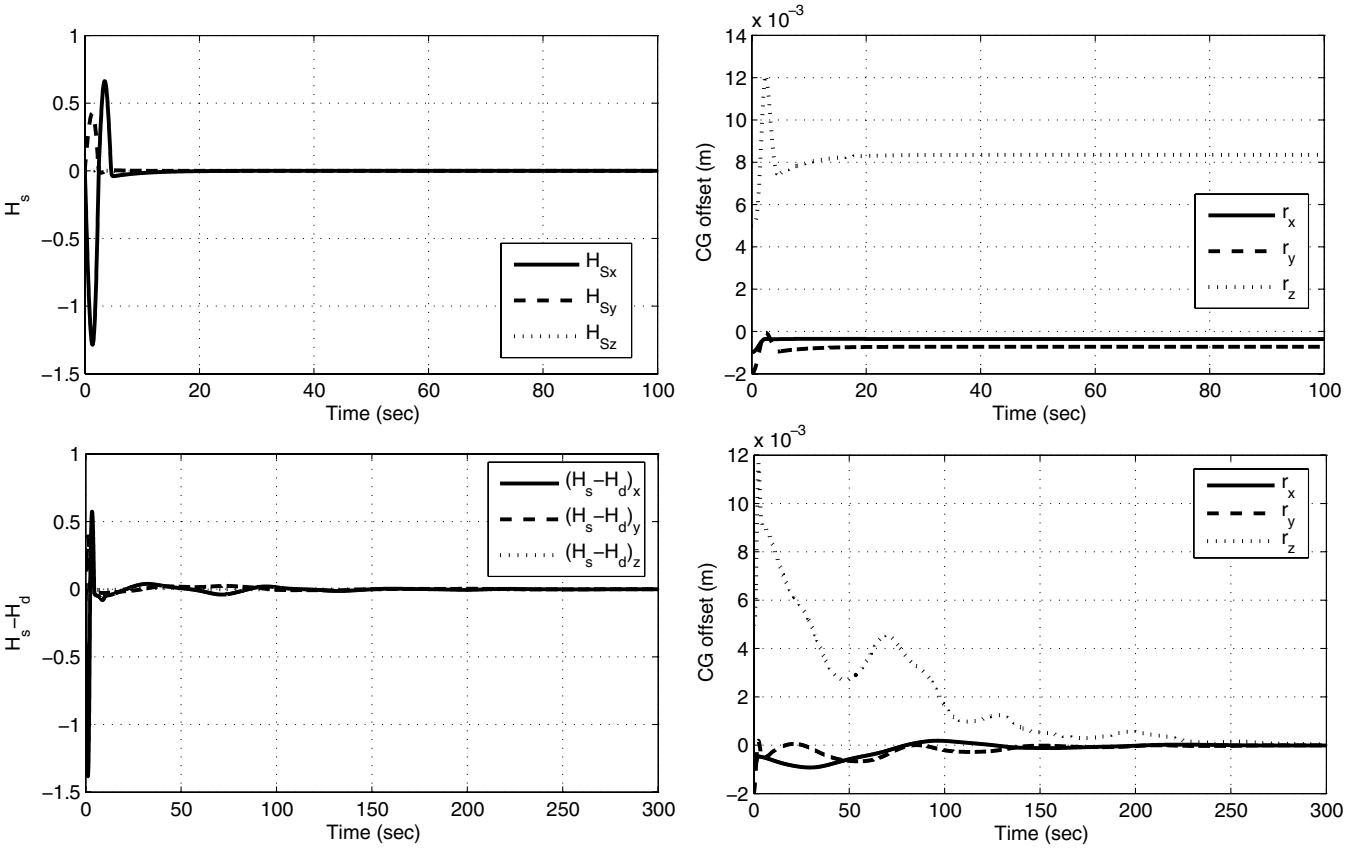

Fig. 3 Adaptive mass balancing control simulation results.

mass balancing control simulation without persistent excitation of the simulator. The angular momentum of the spacecraft (shown in the top left plot) becomes zero as the center of mass offset is compensated using the adaptation law. However, the converged center of mass offset (shown in the top right plot) does not show the correct results. The resulting center of mass becomes the null space solution of the matrix $[\mathbf{g}\times]$. With persistent excitation (shown in the bottom plots), the tracking error becomes zero and the center of mass offset also becomes zero. This shows that the persistent excitation during the adaptive control of the automatic mass balancing system is important.

V. Naval Postgraduate School Bifocal Relay Mirror Spacecraft Simulator

The concept of the BRMS is to redirect laser light from ground-based, aircraft-based, or spacecraft-based lasers to distant points on the Earth or in space. The BRMS uses two optically coupled telescopes. The receiver telescope captures the incoming laser beam and the transmit telescope directs the beam to the desired target point. To test and verify control techniques for this fine attitude control application using a ground-based spacecraft test bed, external disturbances, including the gravity disturbance, should be minimized.

The experimental test bed developed at the Naval Postgraduate School for simulations of the BRMS is shown in Fig. 4. The spacecraft simulator is supported by a spherical air bearing to allow rotations about three axes. The ball of the spherical air-bearing system is 10 in. in diameter and requires approximately 70 psi to float the approximately 800 kg of the simulator. The z axis of the spacecraft body is aligned with the direction of the gravity vector when the spacecraft is maintained at zero attitude. Therefore, the yaw rotation of the spacecraft simulator is not limited, but the maximum angular motion in roll and pitch is limited to around 20 deg with the installed safety bumpers.

Figure 5 shows a schematic of the spacecraft simulator electronics. A single on-board industrial PC (PC104), equipped with serial, analog, and digital I/O ports, serves as the main embedded computer for spacecraft guidance, navigation, and control systems. The on-board computer wirelessly communicates with the host computer via transmission control protocol/Internet protocol. The main simulation loop is operating at 40 Hz and the xPC Target™ toolbox of the Matlab/Simulink® software is extensively used for the real-time spacecraft bus control. The power switching and control electronics module shown in Fig. 5 interfaces with various subsystems including the control moment gyroscope (CMG) control system, the optical top deck gimbal control system, and the automatic mass balancing control system. The CMG control system includes a dedicated controller for each inertia wheel motor and gimbal motor operating at 1 kHz. The dynamics of the gimbal system is ignored in the development because the gimbal rate is kept small during the experiment. For slow maneuvers, the gimbal angle error stays within ± 0.004 rad. The gimbal angle error is mainly due to the delay of 0.025 s in the system.

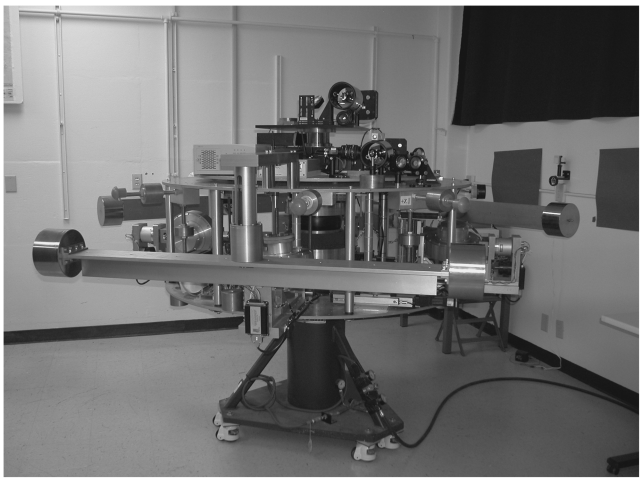

Fig. 4 NPS bifocal relay mirror spacecraft test bed.

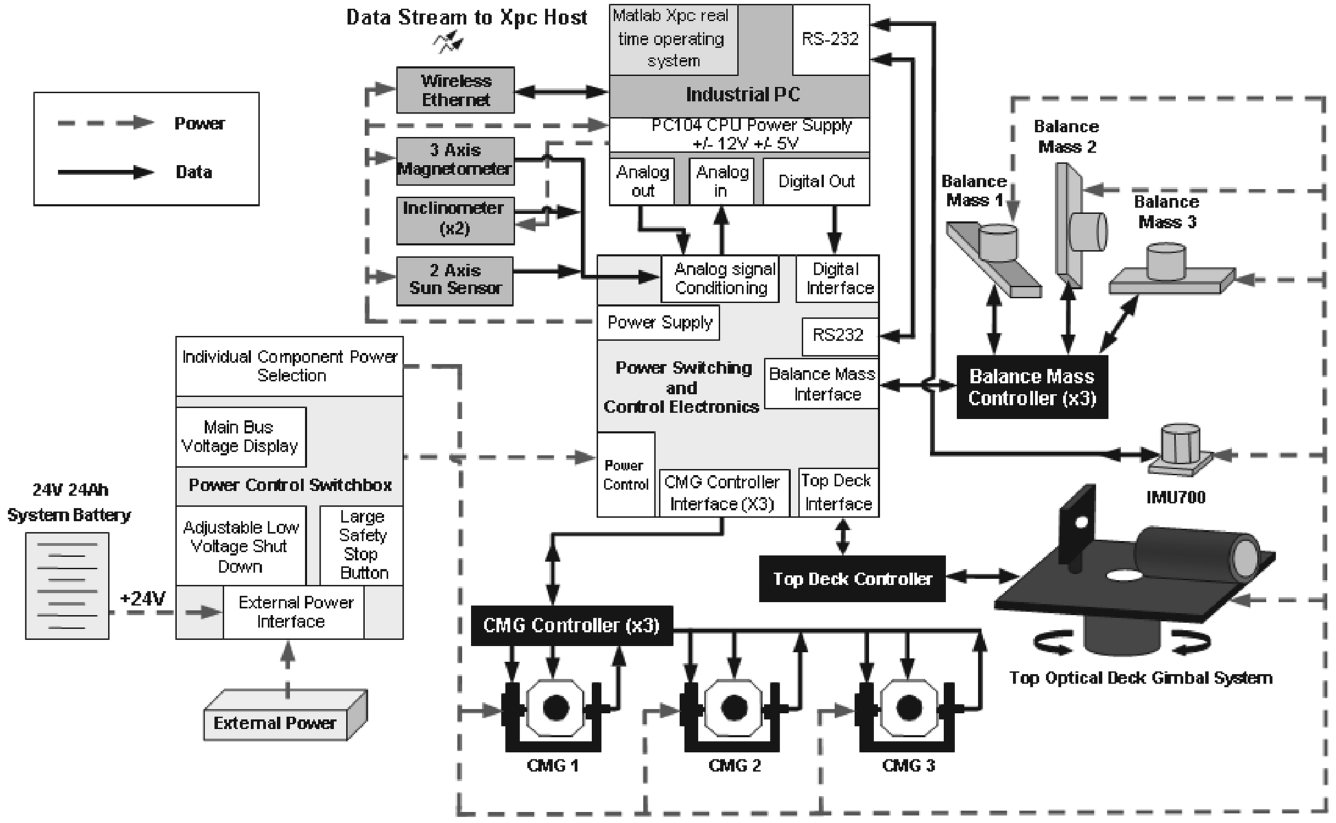

Fig. 5 Schematics of the spacecraft simulator electronics.

The automatic mass balancing control system consists of three linear stages with a dedicated controller for each stage. The linear stages are aligned such that the three balance masses are translated parallel to the three axes of the spacecraft body coordinates. Each linear stage has a maximum travel distance of 15 cm (or ± 7.5 cm) with an accuracy of 18 μm and bidirectional repeatability of ± 5 μm. The linear encoder of the stage has a resolution of 5.2185 μm. The mass value of the balance masses is 10.89 ± 0.01 Kg including the carriage. The dynamics of the mass translation is also ignored in the development because the rate of the center of gravity compensation will be sufficiently small.

Serial communication between the power switching and control electronics and the industrial PC exchanges data from the CMG, top deck gimbal, and automatic mass balancing control systems. The inertial measurement unit (IMU700) built by Crossbow Technology is connected to the second serial port of the on-board computer. The fiber optics rate gyroscopes in the IMU have in-run bias stability of <20 deg/h, bandwidth of >100 Hz, and random walk of <0.4 deg/$\text{h}^{1/2}$. The bandwidth of the current rate gyros integrated into the IMU unit is large enough to detect vibrations created from the CMGs. To minimize the effect of this high frequency noise, low pass filters are applied to the angular rate signals when the angular momentum of the spacecraft is determined. The filtered rate data have a standard deviation of $4.7e-3$ rad/s, $1.2e-3$ rad/s, and $3.7e-3$ rad/s in the x, y, and z axes, respectively. The analog I/O of the on-board computer also interfaces two inclinometers (roll, pitch), a 2-axis (infrared) sun sensor, and a 3-axis magnetometer. The spacecraft attitude is determined by the direct integration of the kinematic equation using the IMU rate data. A star tracker with a better attitude estimation algorithm is currently being developed.

The spacecraft bus also employs three flexible structure simulators consisting of a rotational mass connected through a torsional spring. The flexible structure simulators provide disturbance torques due to the excitation of the flexible body of the spacecraft. The flexible masses are detached from the simulator to minimize the deformation of the structures and to be consistent with the spacecraft equation of motion used for the development of the automatic mass balancing method. Currently, three single gimbal CMGs serve as primary actuators for the spacecraft simulator. The angular momentum of each CMG is rated at 22.5 $\text{N} \cdot \text{m} \cdot \text{s}$ for 2500 rpm. For experiments, the inertia wheel of the CMG is rotating at a constant speed of 200 rad/s. For the BRMS, CMGs are the preferred actuation devices due to the rapid target acquisition requirement and the fine tracking and pointing requirements. The geometric configuration of the CMG array determines the characteristics of the momentum space for the spacecraft control. The current CMG array configuration, shown in Fig. 6, is a pyramid-type configuration with the absence of the fourth CMG. The skew angle denoted as β in Fig. 6 can be adjusted in the spacecraft simulator to reconfigure the momentum space. The torque from the CMG array becomes the time derivative of the total CMG momentum $\dot{\mathbf{h}}$, which can be written in matrix form as

$$\dot{\mathbf{h}} = A\dot{\delta} \tag{41}$$

$$A = H_{\text{CMG}} \begin{bmatrix} -\cos\beta\cos\delta_1 & \sin\delta_2 & \cos\beta\cos\delta_3 \\ -\sin\delta_1 & -\cos\beta\cos\delta_2 & \sin\delta_3 \\ \sin\beta\cos\delta_1 & \sin\beta\cos\delta_2 & \sin\beta\cos\delta_3 \end{bmatrix} \tag{42}$$

where H_{CMG} is the constant magnitude of the angular momentum of each CMG and δ_i is the gimbal angle of the ith CMG ($i = 1, 2, 3$). The

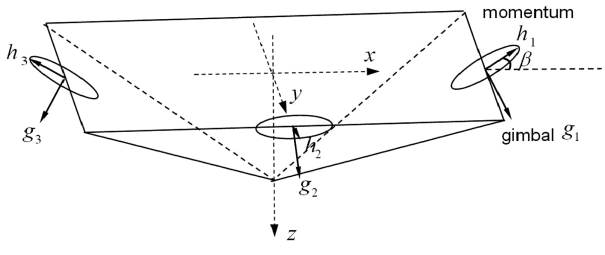

Fig. 6 CMG array configuration of the BRMS simulator.

CMG steering law is a simple inversion of the matrix A such that

$$\dot{\delta} = A^{-1}\dot{\mathbf{h}} \tag{43}$$

The CMG steering law will suffer from a singularity problem when the matrix A is ill conditioned. For experimental verification of the automatic mass balancing methods, it is desirable to avoid singularity states without introducing error in the torque generated from the CMG array. Therefore, the CMG array is configured to have the largest singularity-free momentum volume by adjusting the skew angles of the CMGs. When the skew angle is adjusted to 90 deg, the CMG array provides a singularity-free momentum sphere with the radius of H_{CMG}. The experiment is performed such that the total momentum from the CMG array stays in this singularity-free momentum sphere.

VI. Automatic Mass Balancing Experiments

Before performing mass balancing experiments, all the components on the spacecraft simulator are secured in place to prevent any mass shift during experiments. It is also important to balance any rotational elements on the spacecraft simulator. The CMGs are the main rotating elements of our simulator. To balance the CMGs about their gimbal axes, a laser source is installed on the spacecraft simulator. The impact position of the laser beam is recorded from about 17 m away from the simulator. Then, the mass balancing of each CMG is manually performed using the lead foil tape to achieve a consistent impact position of the laser beam for any gimbal angle when the spacecraft simulator is at the equilibrium state. This CMG balancing process typically takes a very long time. Any unbalance of CMGs will remain as a dynamic unbalance during the experiments.

A batch estimation technique for compensation of the center of gravity offset is first considered for the automatic mass balancing. A sinusoidal reference trajectory is generated and quaternion feedback control is implemented for following the trajectory. The center of gravity is initially located below the center of rotation which provides a stable equilibrium point. With the lower center of gravity position, the center of gravity offset in the x and y axes can be reasonably balanced manually to minimize the momentum buildup and eventual saturation of the singularity-free momentum space during excitation. Figure 7 shows the measured spacecraft angular rate, Euler angles (2-3-1 rotation sequence), and CMG gimbal angles. The recorded angular rate, attitude, and gimbal angles are used for the batch estimation of the system inertia matrix and the simulator mass times the center of gravity vector discussed in Sec. III. The resulting values from the experiment are

$$J = \begin{bmatrix} 130.34 & 3.01 & 10.52 \\ 3.02 & 174.64 & -0.40 \\ 10.52 & -0.40 & 181.23 \end{bmatrix}, \qquad m\mathbf{r} = \begin{bmatrix} 0.00196 \\ 0.00481 \\ 0.19695 \end{bmatrix} \tag{44}$$

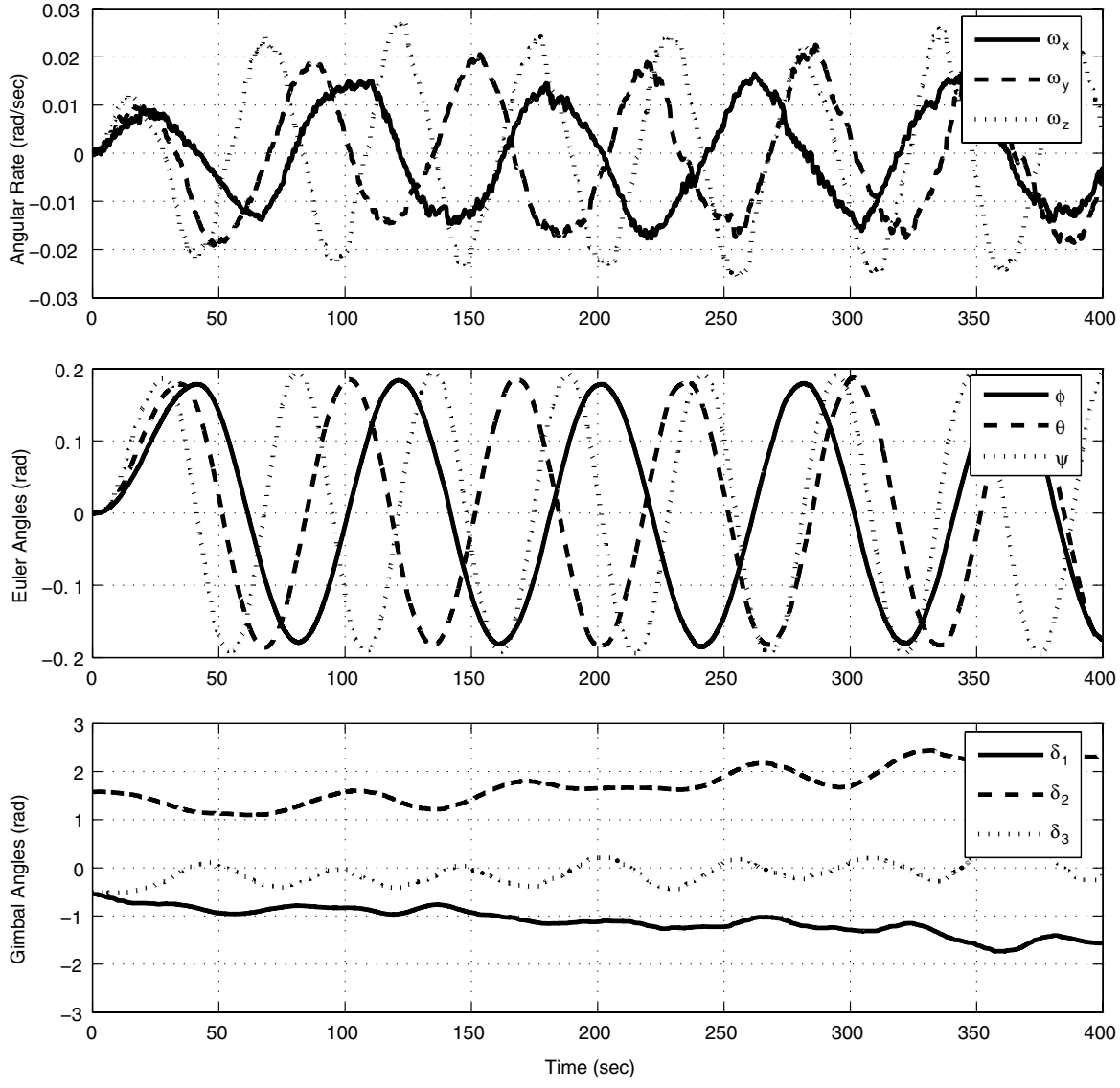

Fig. 7 Experiment data for batch estimation.

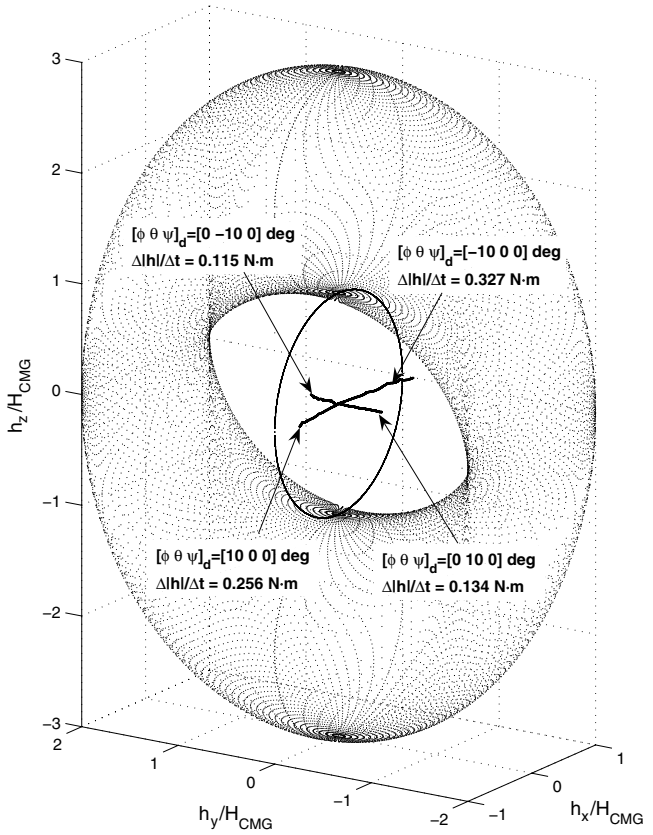

Fig. 8 Momentum trajectories and gravitational disturbances shown in normalized momentum space.

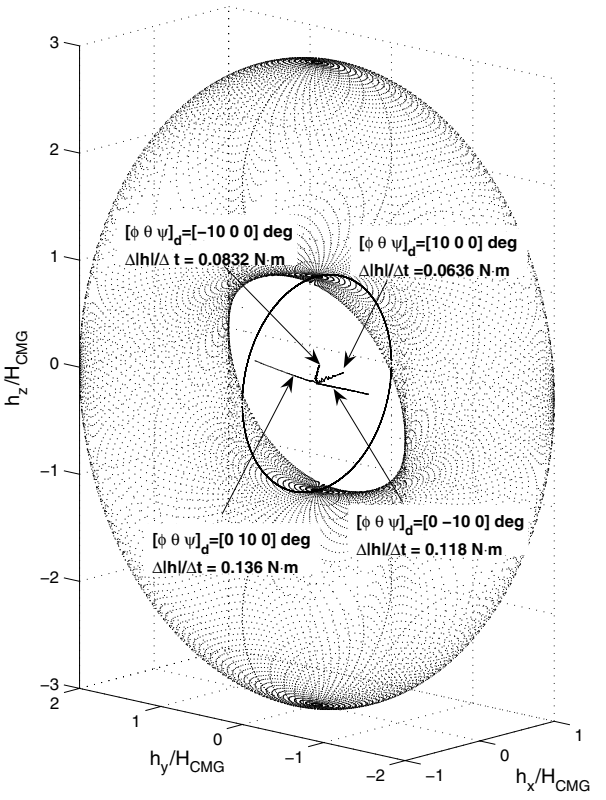

Fig. 9 Momentum trajectories and gravitational disturbances after center of gravity compensation.

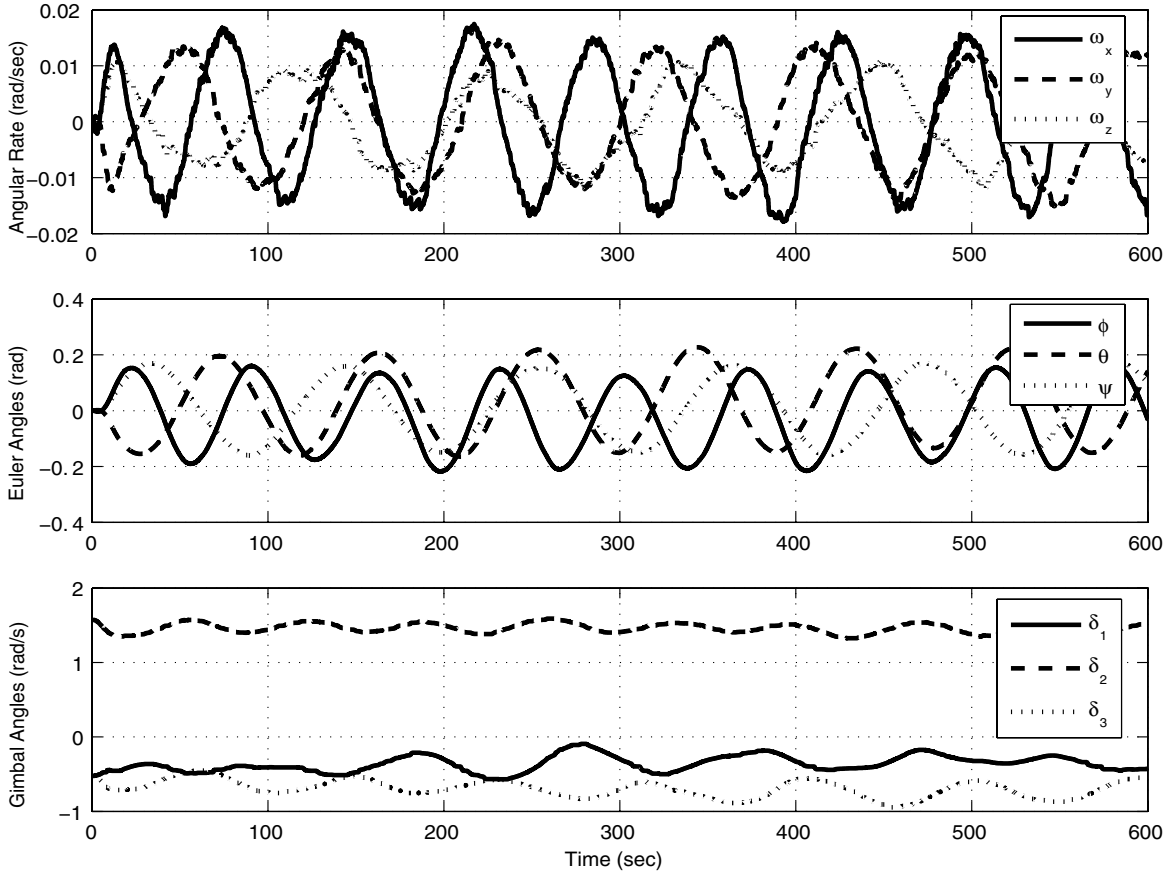

Fig. 10 Spacecraft trajectories and gimbal angles during automatic mass balancing.

Next, the estimated mass multiplied by the center of gravity vector is used to directly compensate for the center of gravity offset using Eq. (17). The required distance of the balance masses for center of gravity offset compensation becomes

$$\Delta d = [-0.00018 \quad -0.00044 \quad -0.01809]^T m$$

Figure 8 shows the plot of the singularity surface and the momentum envelope of the spacecraft simulator using lattice points. Each lattice point represents the momentum state where the corresponding gimbal angle set results in a singular A matrix shown in Eq. (42). The singularity plot has a doughnutlike hole on the y–z plane and a ring on the x–z plane. The momentum magnitude of the plot is normalized by H_{CMG} ($1H_{\mathrm{CMG}} = 16.6\ \mathrm{N \cdot m \cdot s}$) and thus the spacecraft has a singularity-free momentum space with at least $1H_{\mathrm{CMG}}$ in magnitude in any direction from the origin.

Figure 8 also shows the momentum trajectories of the CMG array for 50 s during which the spacecraft simulator is commanded to maintain four different attitudes. The total momentum from the CMG array at the initial time is zero and the spacecraft is oriented to the desired attitude initially to minimize the transient maneuver time. When there are no external disturbances, the momentum trajectories should be constant once the spacecraft reaches the steady state. Without compensation of the center of gravity offset, the gravitational disturbance forces the CMG array to accumulate momentum and eventually saturate the available momentum space of the spacecraft. The gravitational disturbance is determined by the rate of change of the total momentum magnitude of the CMG. In Fig. 8, $\Delta|h|/\Delta t$ represents the average rate of change of the total momentum magnitude once the spacecraft has reached the steady state, which can represent the constant gravitational disturbance torque due to unbalance. The resulting gravitational disturbance shown in Fig. 8 is quite large and quickly saturates the usable momentum space.

Figure 9 shows the momentum trajectories of four different attitudes for 2 min after the balance masses are translated by Δd. The gravitational disturbance is reduced, which can be seen after comparing the new results to the four different attitude values of $\Delta|h|/\Delta t$ in Fig. 8. As shown in [24] with an approximately 200-kg spacecraft simulator, a good manual balancing can reduce the gravitational disturbance torque on the order of magnitude of $0.01\ \mathrm{N \cdot m}$. Although the mass of the NPS simulator (about 650 kg without flexible structure simulators) is heavier, the results with a single estimation do not provide balancing results comparable to a good manual balancing described in [24]. With the initially unbalanced simulator, obtaining good excitation without saturation of the available momentum space is difficult. The estimates of the unbalance vary considerably for each run with different excitation maneuvers, so achieving good excitation is a crucial element for obtaining accurate batch estimation results.

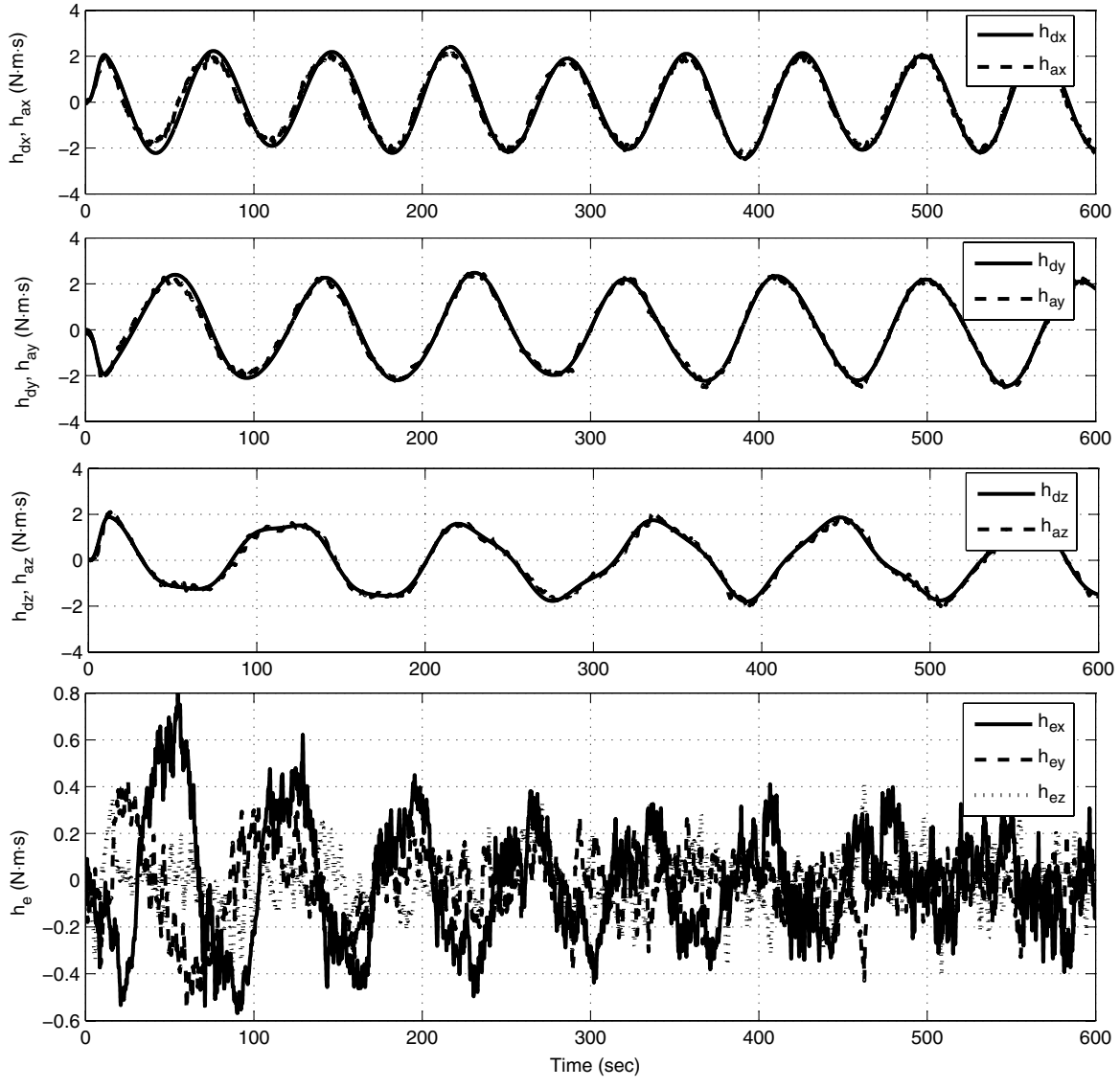

Fig. 11 Desired and actual angular momentum and momentum tracking errors.

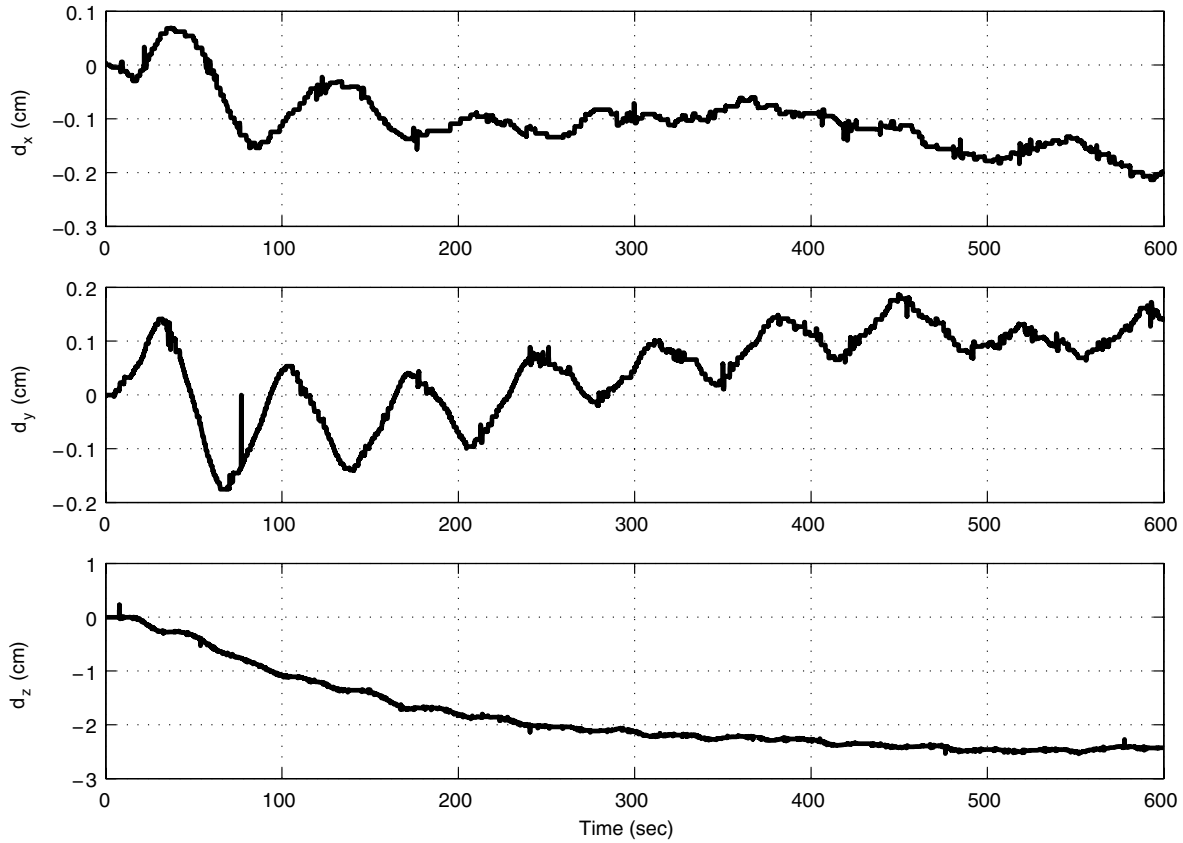

Fig. 12 Position of balance masses.

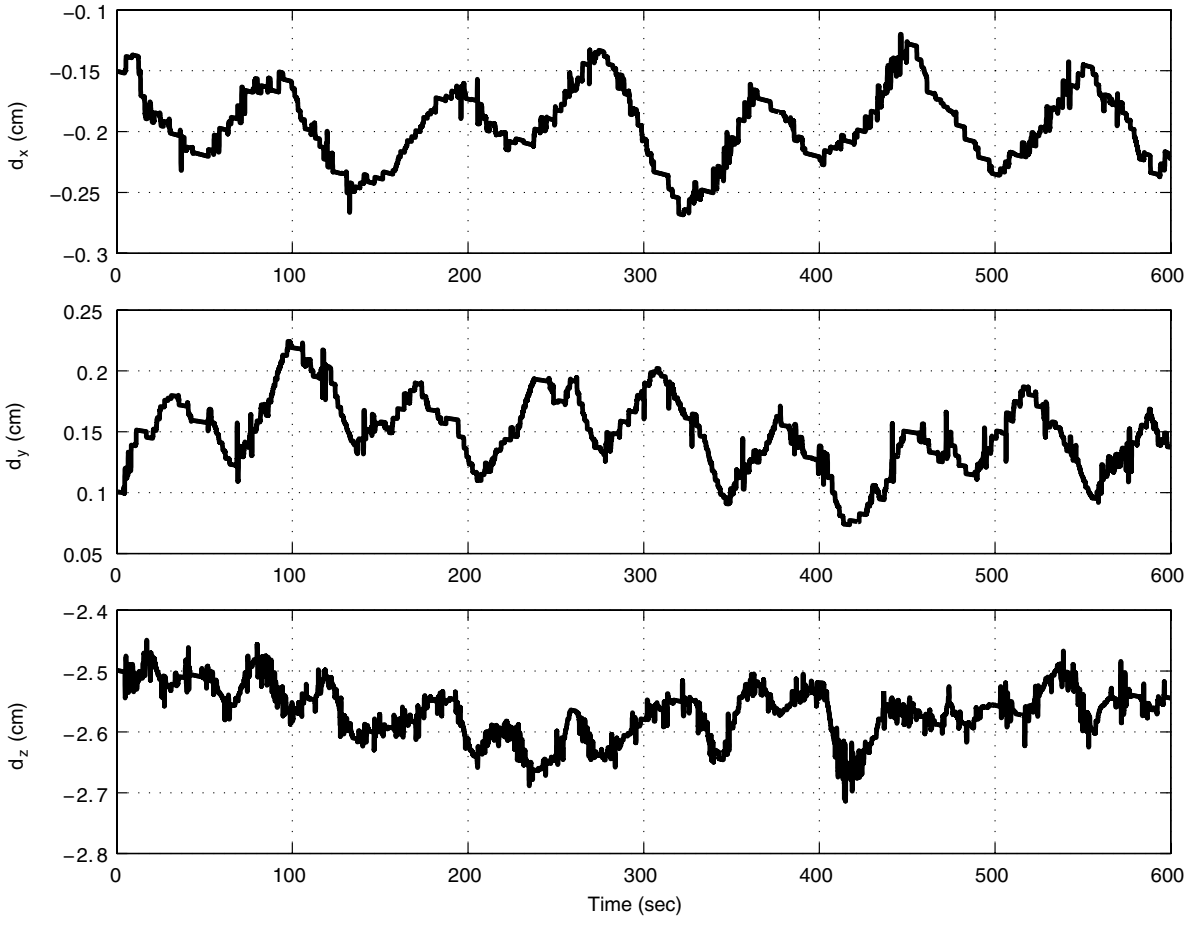

Fig. 13 Position of balance masses with new initial position.

In fact, Fig. 9 represents the best results selected from more than 10 different runs. Applying different estimation algorithms such as filtering and energy balance methods also results in different estimation values. In addition, there are other sources of error including the sensor noise, the misalignment of the balance-mass translation stages, the incorrect measure of the balance masses, and the error in the balance-mass positions. Consequently, repeated estimation is necessary to achieve good balancing results with the batch estimation methods. The verification of the balancing results is also a time-consuming process with the batch estimation. In most cases, the limitation of the simulator rotation in the x and the y axes prohibits the inspection of pendulum frequencies. Therefore, gravitational disturbance is either measured at different attitudes of the spacecraft (such as shown in Fig. 9) or indirectly determined by observing the spacecraft trajectory errors resulting from the unbalance during the specified maneuver.

The next experiment is the proposed adaptive control method. Figure 10 shows the actual spacecraft trajectories as well as the gimbal angles of the CMGs during the adaptive mass balancing experiment. Smooth sinusoidal spacecraft angular trajectories are designed and the corresponding desired momentum trajectories and feedforward control commands are used in the control law. Figure 11 shows the desired and actual spacecraft angular momentum trajectories and momentum trajectory tracking errors. Based on the adaptation law in Eq. (39), the actuation of the balance masses is based on these tracking errors. Theoretically, tracking errors become zero when there are no external disturbances. The momentum tracking errors are noisy when the angular rate measurements are noisy. Therefore, rate sensor noise directly affects the accuracy of the mass balancing. Figure 11 reflects the angular momentum errors using the filtered angular rate signal.

The spacecraft simulator has about ± 15 deg of rotational freedom in the x and the y axes. Accordingly, the angle between the z axis and the gravity vector is within ± 15 deg. The gravitational disturbance due to the z-axis unbalance becomes much smaller than the x- and y-axes unbalance because the magnitude of the cross product is small for a small angle between two vectors. Therefore, the correction of the z-axis unbalance will be much slower than the correction of x- and y-axis unbalance. For the faster convergence, the adaptation gain for the z axis is set to 10 times larger than the gains in the x and y axes during experiments. Because the higher adaptation gain tends to amplify the effect of the sensor noise, very high adaptation gain cannot be used. Another way to enhance the convergence rate is to use a small feedback gain in the control law shown in Eq. (37). With the small feedback gain, the momentum trajectory tracking errors will represent external disturbances more faithfully. However, the spacecraft simulator needs to closely follow the desired momentum trajectory during the balancing process in order to maintain stability and maintain the attitude within the rotational limits of the simulator. Therefore, it is difficult to speed up the convergence rate. In Fig. 11, momentum errors slowly decrease during the 10 min run. The positions of the balance masses shown in Fig. 12 also indicate that the balance masses would continue to converge even after 10 min. Because of the bias of the rate gyros, the spacecraft attitude becomes inaccurate after the long period of experimentation. The corresponding gravity vector measurement also becomes inaccurate and it begins to affect the computation of the adaptation rule. Therefore, the balancing process needs to be restarted. There is also a limit on the amount of on-board memory for data capturing.

Figure 13 show the positions of the balance masses with the new initial mass positions of $d_0 = [-0.15, 0.1, -2.5]^T$ cm. The balance masses are unable to settle to the constant values suggesting that there are disturbance elements other than the static unbalance. The magnitudes of the negative peak to the positive peak are about 0.1 cm for the x and z axes and slightly less for the y axis. Because 0.1 cm actuation of the balance mass can create a maximum gravity torque of about 0.1 N $\cdot$ m, the residual disturbances are quite large.

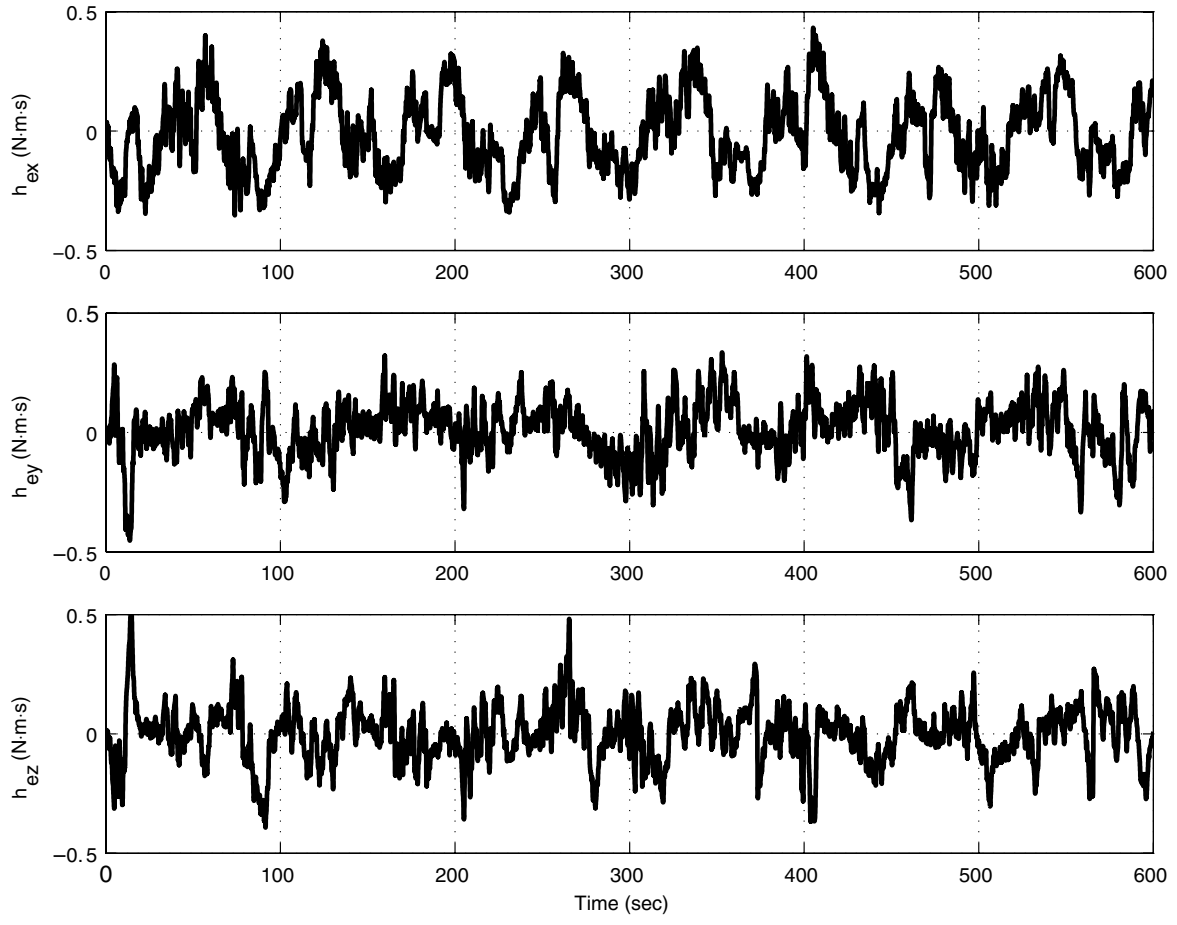

Fig. 14 Angular momentum tracking errors with new initial balance-mass position.

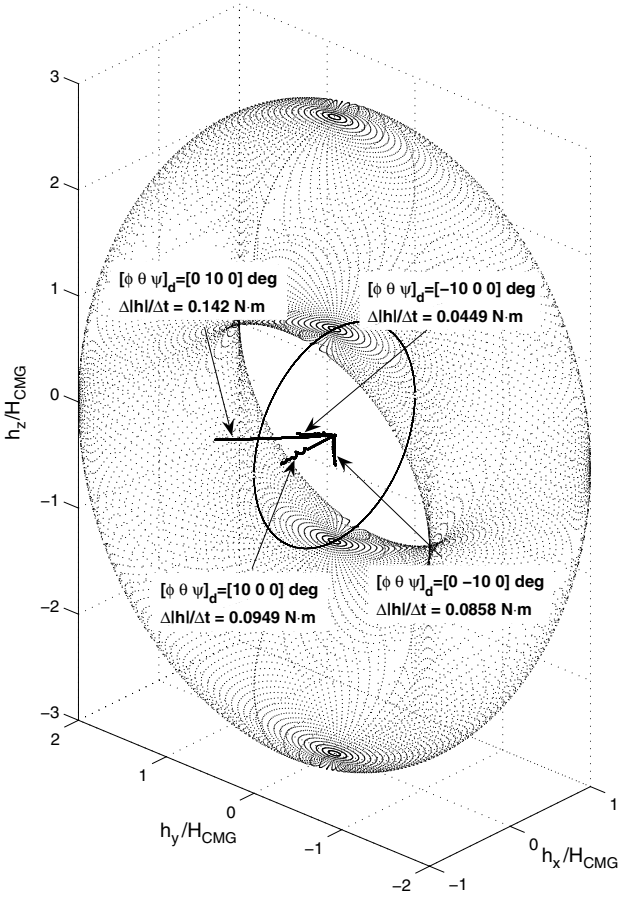

Fig. 15 Momentum trajectories and gravitational disturbances after center of gravity compensation.

Using a smaller adaptation gain may eliminate peaks, but it will also result in a premature stop of the center of gravity compensation. The balancing procedure is usually started from the lower center of gravity location, and a premature stop will result in a pendulum motion at the end of the balancing. During the experiment, the balancing maneuver is kept slow and the relatively high adaptation gain is used for faster convergence. Therefore, the resulting positions of the balancing masses somewhat represent the effort of the residual disturbance compensation.

Figure 14 shows the corresponding angular momentum tracking errors. The peaks of the momentum errors in the x and y axes seem to occur when the spacecraft has reached its maximum or minimum attitude. This suggests that the center of gravity shift due to the structure sagging is a main source of error. The effect of the structure sagging can be minimized by performing a calibration and sensitivity test, which determines the relationship between the simulator tilt and the center of gravity shift. We leave this test as a future work in this paper. The other sources of error, such as environmental torques, are difficult to verify with the given noisy momentum tracking errors.

To verify the balancing results using the adaptive control method, gravitational disturbance torques at four different attitudes are computed again in Fig. 15. For the balance-mass positions, the mean values of the second half of the experiment in Fig. 13 are used. The gravitational disturbances shown in Figs. 8, 9, and 15 are also summarized in Table 1.

From Table 1, the batch estimation method and the proposed adaptive balancing method with the account of static unbalance only show improved but limited balancing performance in the experiment. The results suggest that the consideration of dynamic balancing is inevitable for our spacecraft simulator. To correct dynamic unbalance, the balancing masses need to be actuated during the spacecraft maneuver. However, actuating balance masses during spacecraft simulation will alter the dynamics of a spacecraft, and the control interaction with the spacecraft attitude control system should be carefully considered.

VII. Conclusions

In this paper, a method of compensating for the center of gravity offset with an automatic mass balancing system is investigated. The direct compensation of the center of gravity resulting from the least-squares batch estimation is first considered. Then, the adaptive control method for automatic mass balancing is proposed for online compensation of the center of gravity offset. With the proposed method, sufficient excitation of the spacecraft simulator will guarantee the correct compensation of the center of gravity offset in the simulation. For verification of the proposed method, experiments are performed with the three-axis rotational spacecraft simulator. It is shown with the experiments that the adaptive scheme with online compensation of the center of gravity can be, with some difficulty, implemented on the spacecraft simulator. The experimental results show that the gravitational disturbance is reduced after applying the automatic mass balancing. Because the dynamic unbalance was not considered in this development, the balancing results show limited performance in the actual experiment.

Acknowledgments

The authors would like to thank Mason Peck of Cornell University for providing motivation and insights on the automatic mass balancing problem. The authors also would like to thank Roberto Cristi of the Naval Postgraduate School for helpful discussions on adaptive control.

References

[1] Fullmer, R. R., "Dynamic Ground Testing of the Skipper Attitude Control System," AIAA Paper 96-0103, 15–18 Jan. 1996.
[2] Peck, M. A., Miller, L., Cavender, A. R., Gonzalez, M., and Hintz, T., "An Airbearing-Based Testbed for Momentum Control Systems and Spacecraft Line of Sight," AAS Paper 03-127, Feb. 2003.
[3] Chung, S., Lobosco, D., Miller, D., and Blaurock, C., "Multi-disciplinary Control of a Sparse Interferometric Array Satellite Testbed," AIAA Paper 2003-5433, 11–14 Aug. 2003.
[4] Schwartz, J. L., "The Distributed Spacecraft Attitude Control Systems Simulator: From Design Concept to Decentralized Control," Ph.D Dissertation, Virginia Polytechnic Institute and State Univeristy, Blacksburg, VA, 7 July 2004.
[5] Yang, Y., and Cao, X., "Design and Development of the Small Satellite Attitude Control System Simulator," AIAA Paper 2006-6124, 21–24 Aug. 2006.
[6] Small, D., and Zajac, F., "A Linearized Analysis and Design of an Automatic Balancing System for the Three Axis Air Bearing Table," NASA TM-X-50177, Goddard Space Flight Center, April 1963.
[7] Hatcher, N. M., and Young, R. N., "An Automatic Balancing System for Use on Frictionlessly Supported Attitude-Controlled Test Platforms," NASA TN D-4426, Langley Research Center, March 1968.
[8] Olsen, T., "Design of an Adaptive Balancing System for the Small Satellite Attitude Control Simulator (SSACS)," M.S. Thesis, Utah State University, Logan, UT, 1995.

Table 1 Comparison of gravitational disturbances

Method/attitude ($[\phi \quad \theta \quad \psi]$)	$[10 \quad 0 \quad 0]$ deg	$[-10 \quad 0 \quad 0]$ deg	$[0 \quad 10 \quad 0]$ deg	$[0 \quad -10 \quad 0]$ deg
Before balancing	0.256 N · m	0.327 N · m	0.134 N · m	0.115 N · m
After balancing using batch estimation	0.0636 N · m	0.0832 N · m	0.136 N · m	0.118 N · m
After balancing using adaptive control	0.0949 N · m	0.0449 N · m	0.142 N · m	0.0858 N · m

[9] Young, J. S., "Development of an Automatic Balancing System for a Small Satellite Attitude Control Simulator (SSACS)," M.S. Thesis, Utah State University, Logan, UT, 1998.

[10] Wilson, E., Mah, R. W., Guerrero, M. C., Galvagni, A. E., Wallace, M. A., and Winters, J. L., "Imbalance Identification and Compensation for an Airborne Telescope," *Proceedings of the 1998 American Control Conference*, IEEE, Piscataway, NJ, Vol. 2, 1998, pp. 856–860.

[11] Li, Y.-B., Bao, G., Wang, Z.-W., and Lv, Y.-D., "Dynamic Modeling for Automatic Balancing System of 3-DOF Air-Bearing Testbed," *Journal of Chinese Inertial Technology*, Vol. 13, No. 5, Oct. 2005, pp. 82–86 (in Chinese).

[12] Prado, J., and Bisiacchi, G., "Dynamic Balancing for a Satellite Attitude Control Simulator. Instrumentation and Development," *Journal of the Mexican Society of Instrumentation*, Vol. 4, No. 5, 2000, pp. 76–81.

[13] Prado, J., Bisiacchi, G., Reyes, L., Vicenta, E., Contreras, F., Mesinas, M., and Juarez, A., "Three-Axis Air-Bearing Based Platform for Small Satellite Attitude Determination and Control Simulation," *Journal of Applied Research and Technology*, Vol. 3, No. 3, Dec. 2005, pp. 222–237.

[14] Mittelsteadt, C., and Mehiel, E., "Cal Poly Spacecraft Attitude Dynamics Simulator," AIAA Paper 2007-6443, 20–23 Aug. 2007.

[15] Kim, B., Velenis, E., Kriengsiri, P., and Tsiotras, P., "A Spacecraft Simulator for Research and Education," *Proceedings of the AIAA/AAS Astrodynamics Specialists Conference*, AIAA, Reston, VA, 30 July–2 Aug. 2001, pp. 897–914; also AAS Paper 01-367, 2001.

[16] Jung, D., and Tsiotras, P., "A 3-DoF Experimental Test-Bed for Integrated Attitude Dynamics and Control Research," AIAA Paper 2003-5331, 11–14 Aug. 2003.

[17] Schwartz, J. L., Peck, M. A., and Hall, C. D., "Historical Review of Air-Bearing Spacecraft Simulators," *Journal of Guidance, Control, and Dynamics*, Vol. 26, No. 4, July–Aug. 2003, pp. 513–522. doi:10.2514/2.5085

[18] Smith, G. A., "Dynamic Simulators for Test of Space Vehicle Attitude Control System," *Proceedings of the Conference on the Role of Simulation in Space Technology, Part C*, Virginia Polytechnic Institute and State University, Blacksburg, VA, 20–22 Aug. 1964, pp. 15-1–15-30.

[19] Schwartz, J. L., and Hall, C. D., " System Identification of a Spherical Air-Bearing Spacecraft Simulator," AAS Paper 04-122, 8–12 Feb. 2004.

[20] Keim, J. A., Acikmese, A. B., and Shields, J. F., "Spacecraft Inertia Estimation via Constrained Least Squares," *IEEE Aerospace Conference*, IEEE, Piscataway, NJ, 4–11 March 2006.

[21] Peck, M. A., "Estimation of Inertia Parameters for Gyrostats Subject to Gravity-Gradient Torques," AAS Paper 01-308, 2001.

[22] Tanygin, S., and Williams, T., "Mass Property Estimation Using Coasting Maneuvers," *Journal of Guidance, Control, and Dynamics*, Vol. 20, No. 4, July–Aug. 1997, pp. 625–632. doi:10.2514/2.4099

[23] Wright, S., "Parameter Estimation of a Spacecraft Simulator Using Parameter-Adaptive Control," M.S. Project, Aerospace and Ocean Engineering Department, Virginia Polytechnic Institute and State University, Blacksburg, VA, 2006.

[24] Romano, M., and Agrawal, B. N., "Acquisition, Tracking and Pointing Control of the Bifocal Relay Mirror Spacecraft," *Acta Astronautica*, Vol. 53, 2003, pp. 509–519. doi:10.1016/S0094-5765(03)80011-5